Report No. TE 29-64

Thermo Electron Engineering Corporation, 85 First Avenue, Waltham, Massachusetts 02154

SECOND QUARTERLY REPORT
FOR
SURFACE AND ADSORBATE STUDIES

June 25, 1963, to September 25, 1963

by

D. Lieb
S. S. Kitrilakis
J. H. Weinstein

Contract No. NAS 3-2539

Prepared for

National Aeronautics and Space Administration
Lewis Research Center
21000 Brookpark Road
Cleveland 35, Ohio

Thermo Electron Engineering Corporation, 85 First Avenue, Waltham, Massachusetts 02154

Report No. TE 29-64

SECOND QUARTERLY REPORT
FOR
SURFACE AND ADSORBATE STUDIES

June 25, 1963, to September 25, 1963

by

D. Lieb
S. S. Kitrilakis
J. H. Weinstein

Contract No. NAS 3-2539

Prepared for

National Aeronautics and Space Administration
Lewis Research Center
21000 Brookpark Road
Cleveland 35, Ohio

Approved by: Sotiris Kitrilakis

S. S. Kitrilakis
Research Manager

TABLE OF CONTENTS

LIST OF FIGURES

CHAPTER I
INTRODUCTION

This program is concerned with experimental studies of the emission characteristics of monocrystalline and polycrystalline thermionic converter electrode materials. The effects of cesium, cesium fluoride, and cesium chloride environments upon the work function distribution of the surface, under various conditions of coverage, is the major area of interest. Another variable is the type of surface preparation given the surface.

The experimental work makes use of scanners which are unique in that they allow scanning to be performed on surfaces which are in equilibrium with the plasma environment. Two types of scanners have been developed at Thermo Electron. One is a photoelectric scanner suitable for low temperatures where thermionic currents are small. The other is a thermionic scanner for high surface and cesium reservoir temperatures where thermionic currents are significant.

One scanner of each type was fabricated for this program after design changes had been made to accommodate the addition of the reservoir required to contain the additives.

CHAPTER II

SUMMARY

The measurements taken of the emission from a polycrystalline molybdenum surface, using a photoelectric scanning device are described in Chapter III. The measurements have been made with cesium only in the tube and then repeated with cesium plus cesium fluoride. The data has been correlated along Rasor plots (ϕ versus T/T_R) and it has been shown that the fluoride additive causes the same type of shift in the value of T/T_R when ϕ goes through a minimum, as has been observed in converter testing with additives. Since the two measurements are based upon completely different types of experiments, the parallelism of the results is of considerable significance.

The physical principles involved in photoelectric and thermionic scanning, and in the reduction of the data to useful forms, are described in Chapter III. Numerical examples using actual data are given and the resulting curves have been plotted. The experimental work to be performed during the Third Quarter is described in Chapter IV.

CHAPTER III
RESULTS DURING THE QUARTER

General

Thermo Electron is conducting a two-pronged effort to determine the effect of the addition of cesium halides to the cesium normally used in the vapor converter.

One approach is based upon an overall engineering program which consists of the fabrication and operation of converters, first with cesium only and then with cesium plus chosen additives. That program has successfully demonstrated a significant improvement in converter performance as a result of the halide presence.[1]

The second approach, which is being pursued under this program, has as its objective a detailed examination of the effects upon converter parameters of the halide additives. Specifically, the following objectives are being pursued:

A. To determine the relationship of the covered-surface work function of the refractory metal electrodes to the temperature of the electrode surfaces, the cesium reservoir temperature, the additive reservoir temperature and other converter variables which appear to play a significant role.

B. To detect and document any preferential adsorption of additives on particular sites or crystals and to relate such effects to covered-surface and bare-surface work functions.

The documentation of a relationship between a number of variables consists of designing and carrying out one or more experiments, which will produce data

from which correlations between the variables may be delineated. Such a program is greatly expedited if theoretical analysis has produced an insight as to the nature of the dependence of the variables in question. Rasor's theory provides this direction in the work under consideration. This theory predicts a unique correlation between the covered work function of an electrode surface and the ratio of the electrode surface temperature to the reservoir temperature (T/T_R). Furthermore, it predicts such a correlation for each value of bare-surface work function. These predictions have been confirmed experimentally by data from a variety of experimenters. The addition of an additive to the vapor atmosphere of the converter introduces the additional variable defined by the additive reservoir temperature.

For the correlation of the effects of cesium halide additives, it has been initially assumed that, when the additive pressure in the tube is held constant, the Rasor theory will continue to be valid; that is, the work function for a particular electrode material will correlate uniquely with the (T/T_R) ratio where T_R is the temperature of the cesium reservoir. This assumption has been substantiated by the converter additives work described above. So far, however, only the dependence of the average work function on the other parameters is documented. It is the aim of this program to investigate the same dependence on a point-by-point basis.

Two available devices are capable of examining electrode surfaces, in the presence of vapors, on a point-by-point basis. Both devices are being employed in the program, and their principles of operation have been discussed in an earlier report.[2] The photoelectric scanner, capable of operating mostly at low temperatures, has been used during the reporting period with a polycrystalline molybdenum surface. This material was chosen since it allows direct comparison with the additive converter work which used molybdenum as the collector

material, thus raising the confidence level in the collector work function correlations. The thermionic scanner, which is capable of higher-temperature operation, is being used initially with a single crystal emitter, and is expected to produce information that will cover both emitter and collector operating conditions.

Photoelectric Scanner

The photoelectric scanner is based upon the measurement of a photoelectric current which is a function of the work function variation of the surface being scanned. It is useful only at low electrode temperatures where thermionic current does not mask the photocurrent. This is the range at which the collector operates in a thermionic converter, which makes the device most useful for studying collector work function. It should also be noted that this device is limited to the determination of work function on a relative scale, since absolute values of work function can be determined photoelectrically only if a monochromatic light source is available. The problem of developing such a source with sufficient intensity to be useful for this work was determined to be beyond the scope of the program. The analytical techniques which are used to convert this relative information to a more useful form will be described later in this chapter.

The photoelectric test vehicle has been completed and is currently being used to scan the polycrystalline molybdenum surface. Figure 1 is a photograph of the emitter structure which consists of the molybdenum test surface, the tantalum sleeve which supports it, and a radiator. The body shell with the collector leadthrough and guard ring is shown in Figure 2. In Figure 3, the test surface can be seen through the sapphire window, and Figure 4 shows the device mounted on the test stand under vacuum. The cooling coil and electrical shielding

are visible. The coil at the top of the bell jar is used to counteract the magnetic field of the heaters.

The molybdenum test piece was carefully prepared so as to insure large grains for study in the scanner. A slice was cut from high-purity molybdenum bar stock and machined to the proper geometry for attachment to the tantalum support. The face was then machined flat to a very close tolerance and cleaned before firing in vacuum at 2200° C for 30 minutes. Heating was accomplished by placing the specimen in a tantalum bucket within the field of an rf coil. Vacuum of the order of 10^{-6} torr was maintained by an oil diffusion system equipped with a liquid nitrogen cold trap. Considerable grain growth occurred, as shown by the general view of the test piece in Figure 5. Figure 6 shows the tooling marks and fine structure of the surface at a magnification of (560x).

Three notches were then filed in the edge of the emitter to serve as a locating aid when taking photographs, and the test piece was electron-beam welded to the support structure.

The cesium and additive reservoirs are on opposite sides of the tube, below the cooling coil. The cesium is contained initially in a glass capsule and distilled into the tube after outgassing has been accomplished. Since testing with pure cesium had to be accomplished before releasing the additive, a special additive capsule was required. The capsule used in this device consists of two pieces of 3/16-inch copper tubing brazed to a short piece of molybdenum tubing. One piece of copper was pinched off and several grams of cesium fluoride were placed in the capsule. After outgassing at 125° C until a low pressure (10^{-6} torr) was obtained, the other copper tube was pinched off. The moly tubing is very brittle and is fractured easily inside the additive tubulation when the cesium fluoride is to be released. A photograph of the capsule is shown in Figure 7.

The scanner may be characterized as a constant current source. Therefore, the output voltage is dependent upon a high-resistance insulator between emitter and collector structures. When the scanner had been assembled, outgassed and charged with cesium, measurement showed that the internal resistance was low. It was suspected that the cause of the low resistance was cesium deposited on the insulators; therefore, the tube was heated to drive off the cesium. This was partially successful, but considerable electrical filtering was still necessary to overcome the noise. A display picture, obtained from the scanner, is shown in Figure 8. The reduced emission produced by the collector wires is clearly visible. The low leadthrough resistance affected the definition of the display pictures; however, the single-line cross-scans were not affected, and the data produced in that manner has been very effective.

Analysis of Results (Photoelectric Scanner)

Display photographs, of which Figure 8 is typical, are extremely useful in identifying the overall features of the surface under examination, and in perceiving the dependence of emission on the local features of the surface as defined by metallurgical examination. However, quantitative measurements cannot be obtained from such photographs. For this purpose, single-line cross-scans are far more suitable. Figure 9 is typical of a series of cross-scans, each of which is obtained by scanning over the same chord on the face of the test piece. In fact, a cross-scan is a plot of current versus position on the test piece. On the same figure, a calibrating signal is also recorded (lower plot of Figure 9). This signal is the output of a standard photocell, onto which the beam used to scan the test piece is directed. The phototube output is connected across the scanner leadthrough. Thus the output of the scanner and the phototube see the same resistance, and any changes in the light source or in the leadthrough resistance affect both outputs and are automatically compensated for.

Before describing the relationship between the observed current values along the scan of Figure 9 and the work function values of the surface, it is well to discuss the physics of this relationship. Figure 10 is a plot of the relative electron current emitted by a surface of work function ϕ when photons of a given energy strike this surface. The work function of the surface is identified on the energy scale. It may be observed from this figure that photons of energy less than ϕ will not result in electron emission, while photons of energies slightly greater than ϕ will yield a given number of electrons independent of the actual photon energy (as a first approximation). As the energy of incident photons increases further, the actual number of electrons yielded decreases. For our purposes, however, we can assume that photons of energies less than ϕ yield no electrons whatsoever, while all photons greater than ϕ yield the same number of electrons. This assumption is shown by the dotted straight lines in Figure 10.

In the photoscanner experiments, a xenon lamp is used, and the characteristic of this lamp is shown in Figure 11. This figure is a plot of the relative number of photons versus the energy level. The curve of Figure 11 has been integrated, and the results are shown in Figure 12, which is a plot of the relative number of photons which have energies greater than E electron volts. Based on the assumption of Figure 10 and the relationship shown in Figure 12, we can state that the currents yielded by the incident photons will be inversely proportional to the work function of the surface within the range of 1.2 to 4.3 eV. Surfaces with work functions less than 1.2 electron volts will emit the same amount of current no matter what their work function when this light strikes them, while surfaces of work functions greater than 4.3 electron volts will emit no current at all. A surface having a work function of 3.5 volts will emit half the current of that emitted by a surface having a work function of 2.92 volts,

since 20% of the incident photons have energies greater than 3.5 electron volts, and 40% of the photons have energies greater than 2.92.

Figure 13 shows a series of plots, each of which relates relative photocurrent to T/T_R (ratio of test piece surface temperature to cesium reservoir temperature) for a particular additive reservoir temperature. These plots are obtained in the following manner. The scanner was operated by holding the cesium reservoir temperature at a constant value, in this case, $T_R = 330° K$. The additive temperature was also held at a constant value, for example, $T_{additive} = 350° K$ for curve B. The molybdenum test piece surface temperature is then established at a given value, time is allowed for equilibrium to be established, and a cross-scan such as Figure 9 is made. The surface temperature is then varied by 50° and another cross-scan is made. This process is continued until a sufficient range of T/T_R has been covered. The data is then analyzed by choosing a specific point such as point A of Figure 9 (which is located near the edge of the test disc), and the current corresponding to that point is recorded and plotted as a point on curve B of Figure 13. This procedure is followed for each of the cross-scans in the series, so that curve B of Figure 13 represents the current at point A of Figure 9 over the range of T/T_R which is of interest. It can be seen that this current rises as the surface temperature (T) is increased until it reaches a maximum. Further increases in surface temperature then cause a decrease in the current. The shape of this curve is essentially the inverse of the relationship of the surface work function ϕ and indicates that ϕ goes through a minimum at the T/T_R ratio where the current goes through the maximum. Table I shows the actual computations which are required to plot a single curve of Figure 13. These particular calculations correspond to curve A of Figure 13, which was obtained with cesium only in the converter. Subsequently, the additive capsule was opened, and its

temperature was raised slowly. A series of scans was made with $T_{add} = 350° K$, which is slightly higher than the cesium reservoir temperature ($T_R = 330° K$) and practically the minimum additive temperature which can be employed. The results are plotted as curve B of Figure 13. A comparison of curve B with the cesium-only case (curve A) shows that only a very minor change has occurred in the T/T_R value at which the maximum current (minimum ϕ) is recorded.

Curve C was then produced by performing the same analysis on a series of cross-scans taken with the additive reservoir temperature at 400° K. Here the peak current (minimum ϕ) has shifted to much higher values of T/T_R. In fact, no minimum has yet been reached at the upper limit of T/T_R in our experiments. Curve D, which is a result of scans taken with $T_{add} = 500° K$, shows a maximum current (minimum ϕ) at $T/T_R = 1.95$, which is a lower value of T/T_R than the cesium-only case.

It should be noted here that the value of relative current is of no significance but that the important feature is the value of T/T_R at which each curve peaks.

In Figure 14, all of the curves of Figure 13 have been converted to a relative work-function scale and normalized to a value of one (1) for the minimum-work-function point. In addition, the results obtained from work-function measurements in the converter are shown in this plot for the cesium-only case and the additive case. The shift of the minimum work-function point to lower T/T_R values, established by converter additive experiments, is thus confirmed by the initial scanner results. The actual location of this minimum on the T/T_R scale appears to be different for each of the two types of experiments, but this may well be due to the significantly lower surface temperatures used in the scanner experiments. The fact that these two methods agree in the trends exhibited by the results is quite significant, since the principle involved in each method of

experimentation is quite different. The measurement performed in the converter depends upon a collection of low-energy electrons, while the scanner, of course, depends on the photo emission from the same surface.

An additional phenomenon which has been revealed by the experimental work is that of time dependence of the additive effect. At temperatures up to 400° K, there appears to be no significant delay effect, as shown by the fact that curve C of Figure 14 is a composite of data taken after 3 hours and 24 hours at temperature, and the two sets of data coincide to a high degree.

Once the additive reservoir temperature has been raised to a high temperature (approximately 500° K), however, a very significant lag time became apparent in that, several days after the temperature was reduced to 350° K, the effect of the additive had not been reduced to its original 350° K effect. This is demonstrated by curve G of Figure 14, which was taken at $T_{add} = 300°$ K.

TABLE I

T °K	T/T_R	I_C Calibrate Amplitude	I_o Photocurrent Amplitude (location 52.5)	Relative Current = $\frac{I_o}{I_C}$
454	1.37	33	43.5	1.32
460	1.39	27	34.5	1.28
580	1.75	24	36.0	1.50
685	2.03	30	53.5	1.78
728	2.15	30	50.0	1.67
825	2.45	38	55.5	1.72
907	2.68	35	56.0	1.60
948	2.80	34	53.0	1.56

Thermionic Scanner

The thermionic scanner permits studies of the emitter work function under conditions which very closely simulate those of an actual converter. The use of this device to study the effects of additives on the emitter has been delayed by past difficulties in assembly of the scanner, and testing will be initiated during the third quarter. Therefore, the third quarterly report will contain a detailed discussion of the thermionic scanner and the method of taking and analyzing the data.

The first emitter to be used in the thermionic scanner will be made of tungsten which is termed single-crystal ⟨110⟩. In fact, this material is not a single crystal but consists of several large grains with a nominal ⟨110⟩ orientation. In order to fabricate the emitter, a disc of this type of tungsten, 80 mils thickness, was brazed (with niobium) to a molybdenum disc which was in turn brazed to a tantalum slug. For location purposes, three notches were made in the edges of the tungsten. It was then electropolished and etched in alkaline potassium ferrocyanide. Finally, it was fired at 2000° C for 10 minutes. Photomicrographs were taken before and after firing. The emitter piece was then electron-beam welded to its support structure.

Figure 15 is a general view of a portion of the emitter at (5x) showing the notches and sub-grain boundaries. The change in visual appearance across grain boundaries may also be seen. This photomicrograph was taken before firing. Figure 16 at (310x) was also taken before firing and shows the different types of surface texture developed by the etch on adjacent sub-grains. In one corner, a blemish left over from electropolishing may be observed. Figure 17 shows an area similar to the one in Figure 16, but after firing in vacuum for 10 minutes at 2000° C. Most of the surface texture developed by etching has been smoothed out.

The test vehicle for the thermionic scanner has been re-assembled. A few minor modifications in design have been made to minimize any strains on the sapphire window which might have led to leaks experienced earlier. In addition, a new lot of windows were obtained. The device is now ready for outgassing after having been leak-checked carefully at the various assembly stages.

Method of Analysis of Thermionic Scanner Results

The thermionic scanning will be performed during the third quarter. For the purpose of illustrating the type of results which are expected and the techniques of interpreting the data, reference will be made to previous work involving thermionic scanning. This work was performed by Thermo Electron under contract to JPL for NASA and has been previously reported.[3,4] Figures 18, 19 and 20 are reprinted from the recent Gatlinburg paper by Rasor, Kitrilakis and Lieb. These figures were obtained during the scanning of a special four-quadrant test surface made up of four tungsten sectors, as illustrated in Figure 20. The quadrant designated P is polycrystalline tungsten, while the others are single-crystal tungsten with ⟨110⟩, ⟨111⟩ and ⟨100⟩ orientations.

Figure 18 is representative of the display pictures obtained during scanning of the test surface. In this picture the bright areas correspond to the regions of high emission and therefore low work function, and, conversely, the dark areas represent regions of low emission and high work function.

Cross scans are plots of current vs position along a single line across the test surface. This line is scanned by fixing the magnitude of one cross field while the other is varied. Figure 19 is a typical series of cross scans obtained from various lines across the surface described above and shown by the display picture of Figure 18.

Cross scan data can be converted directly to numerical results through calculations which make use of the geometry of the test vehicle and the absolute current collected by the probe. The cross scan is calibrated by introducing a known constant current in the probe circuit. As in the photoelectric scanner, the calibration current sees the resistance of the scanner ceramic seal, thus automatically compensating for any changes in the lead resistance.

A sample calculation of work function variation with T/T_R is illustrated in Table II.

TABLE II

T/T_R	T °K	Probe I = total current collected ma	Probe J ma/cm^2	Work Function ϕ eV
2.37	995	1.75	39	1.88
2.49	1043	1.52	34	1.98
2.55	1070	1.70	38	2.03
2.67	1116	0.47	10.5	2.25

The probe hole diameter is 3 mils, and the area 4.5×10^{-5} cm^2. ϕ is calculated using Richardson's equation:

$$J = A T^2 \exp\left(-\frac{\phi}{kT}\right)$$

where T = specimen surface temperature

J = current density collected by the probe

A = 120 $a/cm^2 - deg^2$

Table II results may be plotted on the Rasor work function curves and compared with theoretical results. Changes produced by the addition of cesium fluoride are evidenced by shifts from the pure cesium curves.

Figure 20 shows three sets of data plotted in this manner. Each set of points (designated by a single geometric symbol) corresponds to a particular location on the test surface.

CHAPTER IV
PLANS FOR THIRD QUARTER

During the third quarter, testing of the polycrystalline molybdenum emitter in the photoelectric scanner will be completed. This testing is now in its second stage. The tests in a cesium-only environment have been completed, and those in the cesium-plus-cesium-fluoride environment have been initiated. After completion of this stage of testing, the molybdenum test piece will be removed from the photoelectric scanner and examined metallurgically preparatory to being inserted in the thermionic scanner for additional experimentation.

Concurrently, the single-crystal tungsten emitter will be tested in the thermionic scanner, first with cesium only and then with cesium plus cesium fluoride.

REFERENCES

1. Thermo Electron Report No. 35-64
Final Technical Report for Converter Additive Studies by S. S. Kitrilakis and J. H. Weinstein, December 1963, Contract No. AF 33(657)-10130

2. Thermo Electron Report No. 45-63
First Quarterly Report for Surface and Adsorbate Studies by D. Lieb, June 1963, Contract No. NAS 3-2539

3. Thermo Electron Report No. 36-64
Final Technical Summary Report for Emitter Crystal Structure Study by S. S. Kitrilakis, et al., January 1964, Contract No. 95 0228/NAS7-100

4. Correlations of Observed Non-Uniform Emission from Surfaces in Cesium Vapor by N. S. Rasor, et al. Presented at the Thermionic Conversion Specialist Conference, Oct. 7-9, 1963, Gatlinburg, Tennessee. Sponsored by IEEE and AIAA.

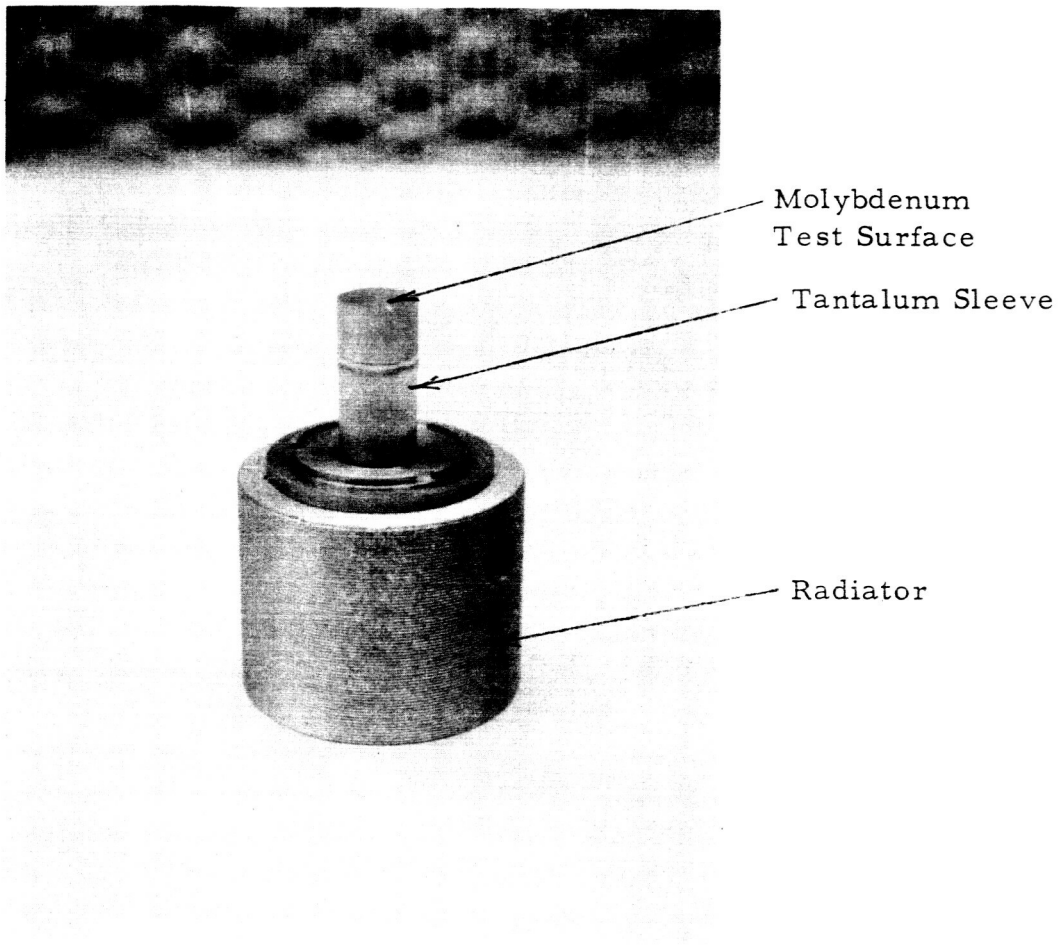

Figure 1. Emitter Assembly (Photoelectric Scanner)

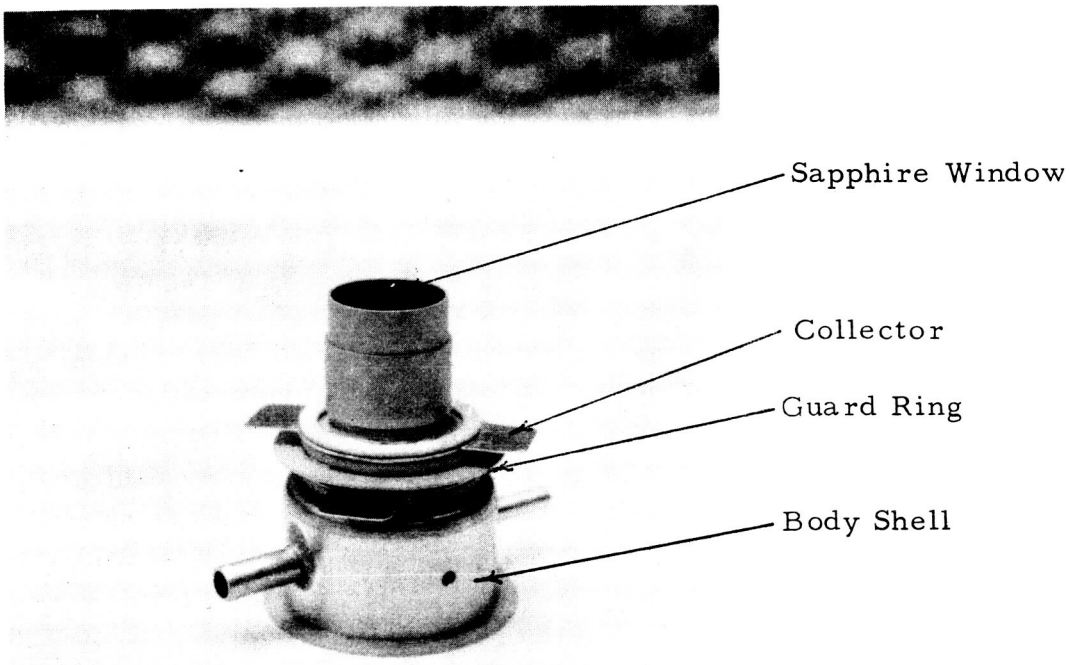

Figure 2. Shell (Photoelectric Scanner)

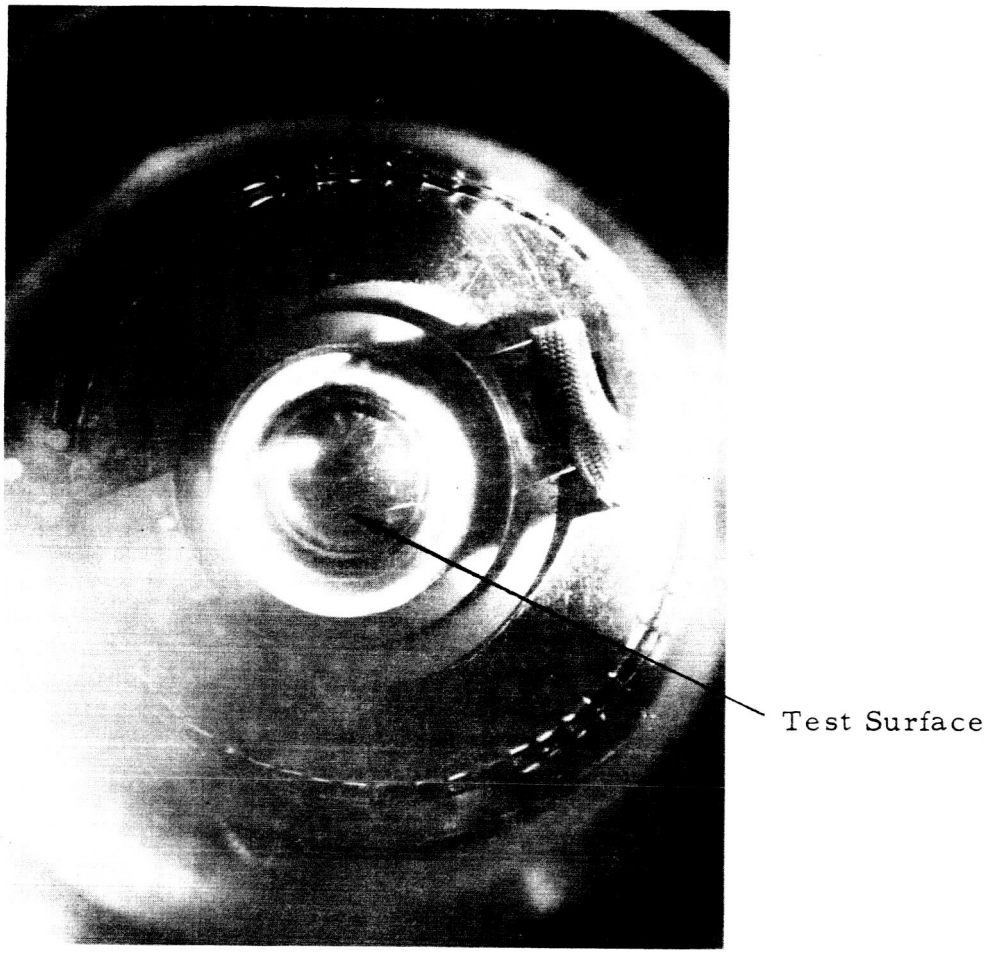

Figure 3. Top View (Photoelectric Scanner)

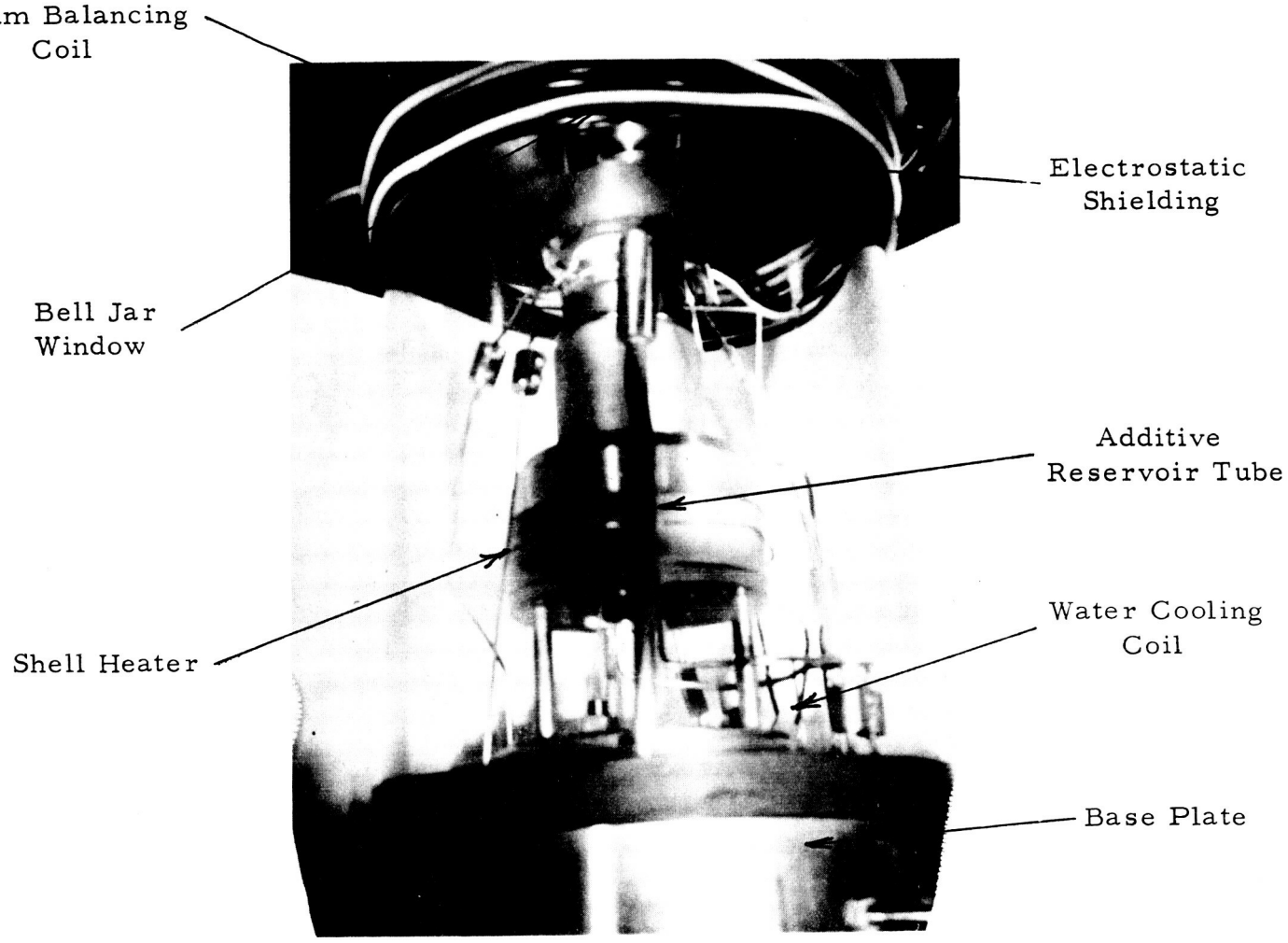

Figure 4. Photoelectric Scanner on Test Stand

Figure 5. Photograph of Molybdenum Surface at (5x)

Figure 6. Photomicrograph of Molybdenum Surface at (560x)

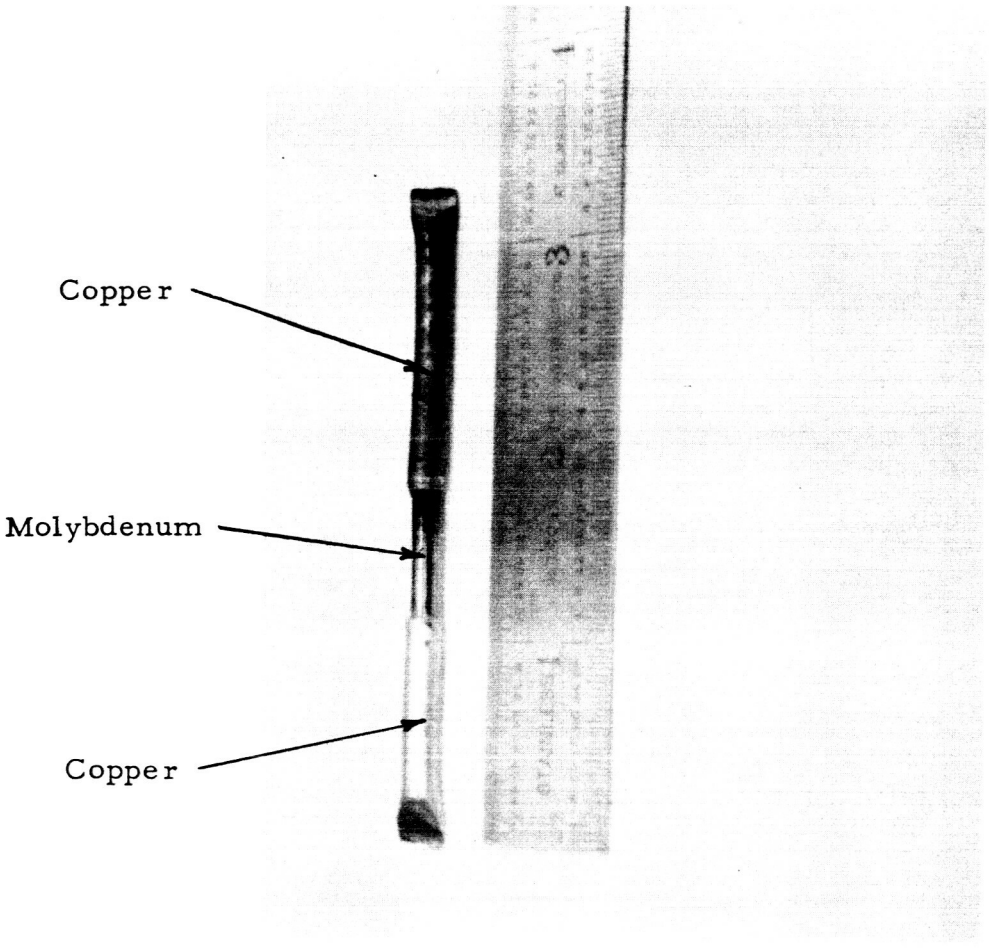

Figure 7. Additive Capsule

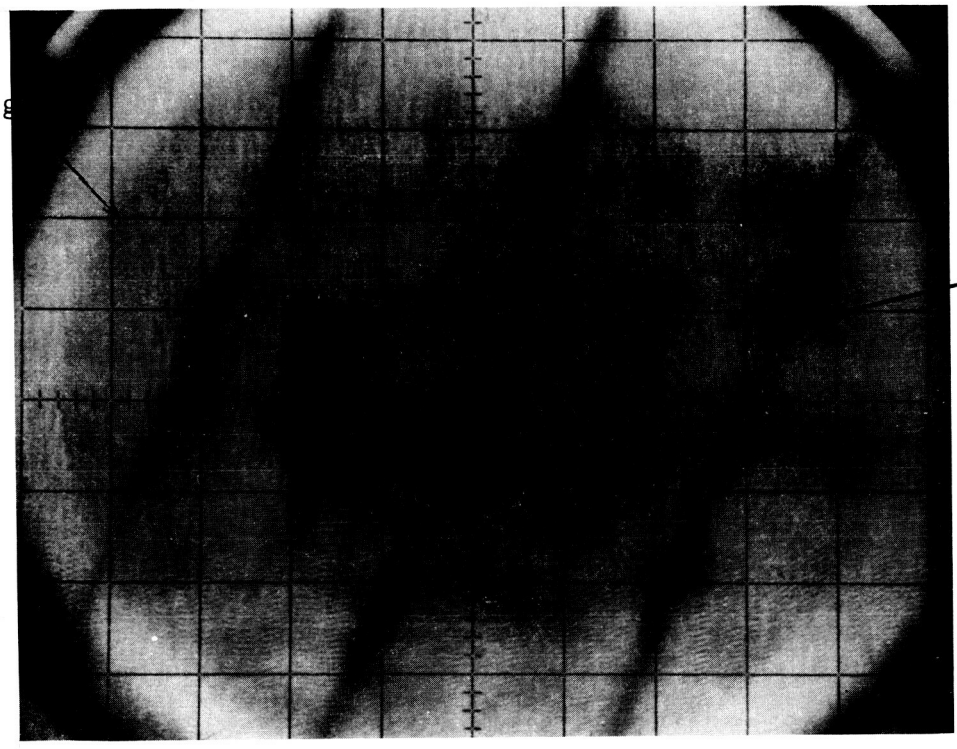

Figure 8. Scanner Display Photograph

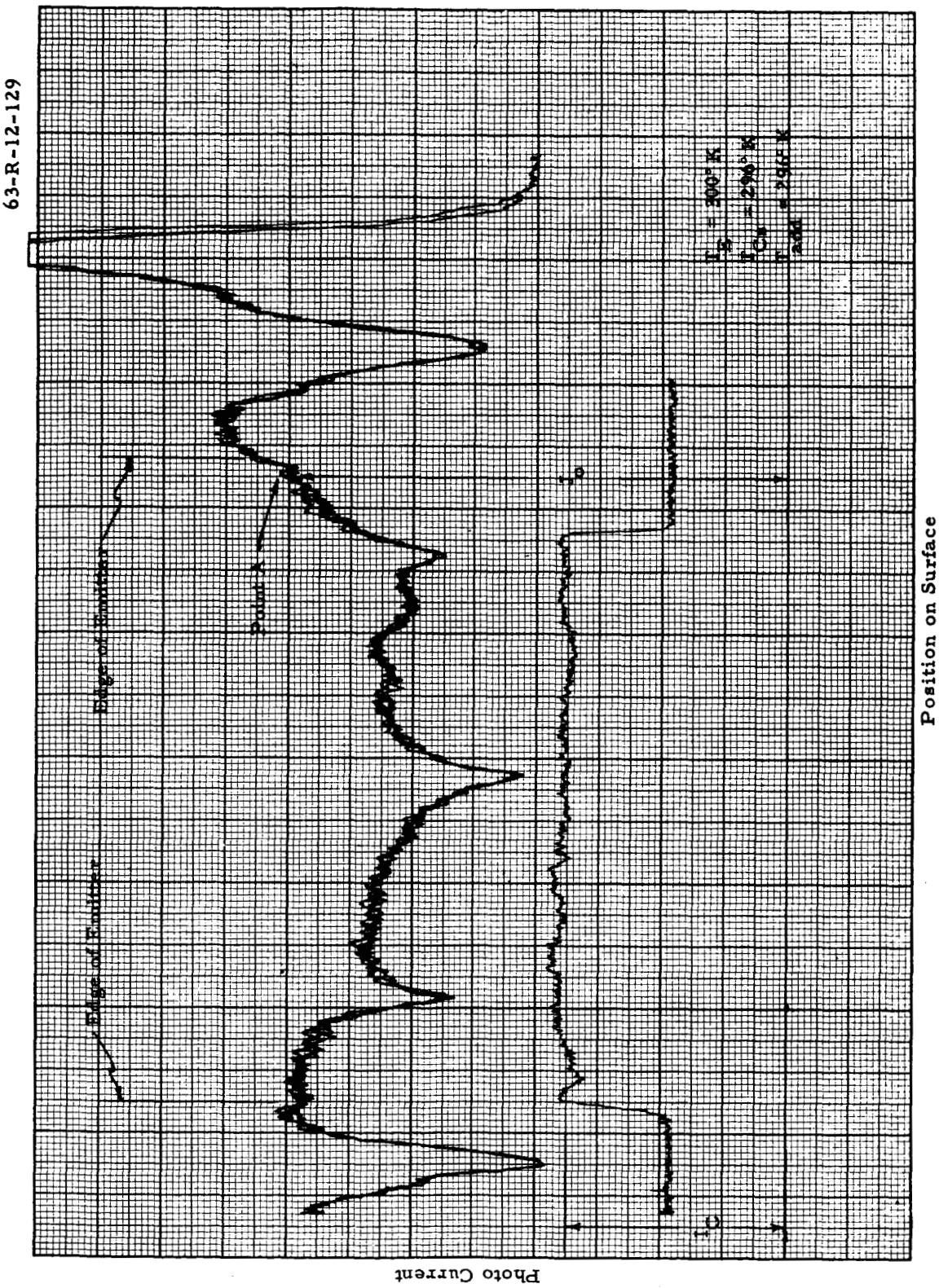

Figure 9. Typical Single Line Cross Scan (Photoelectric Scanner)

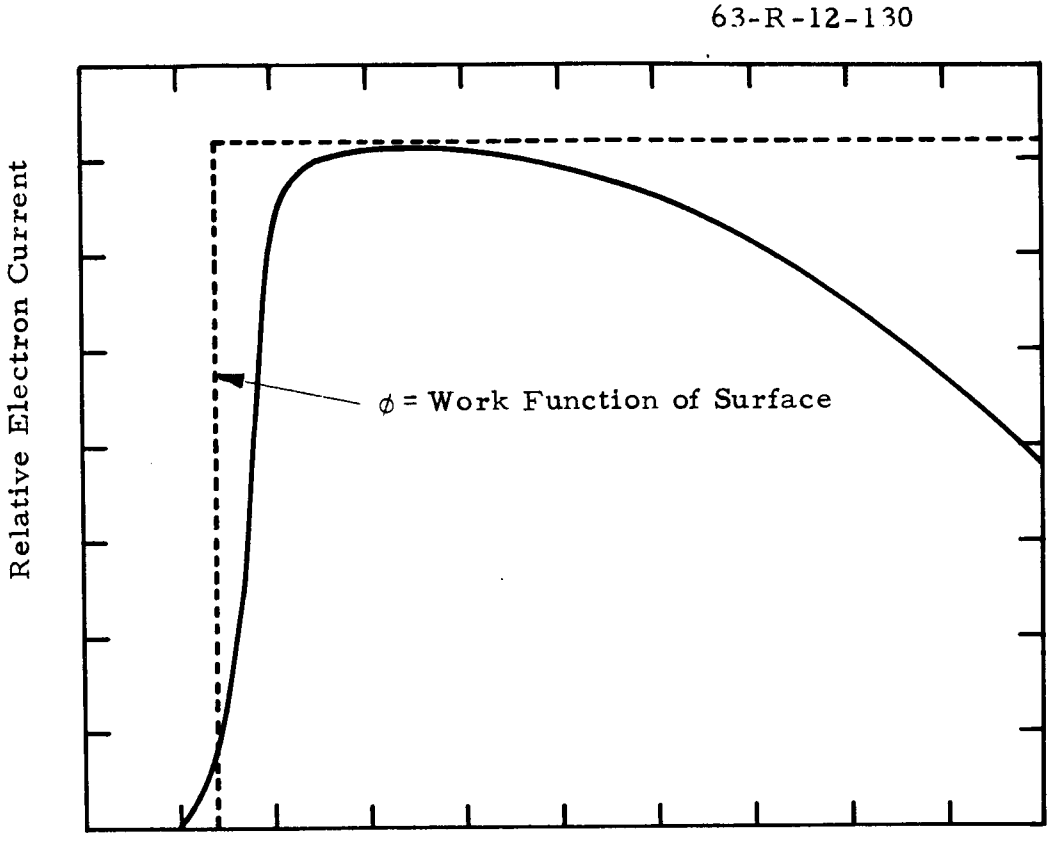

Figure 10. Quantum Effect Plot

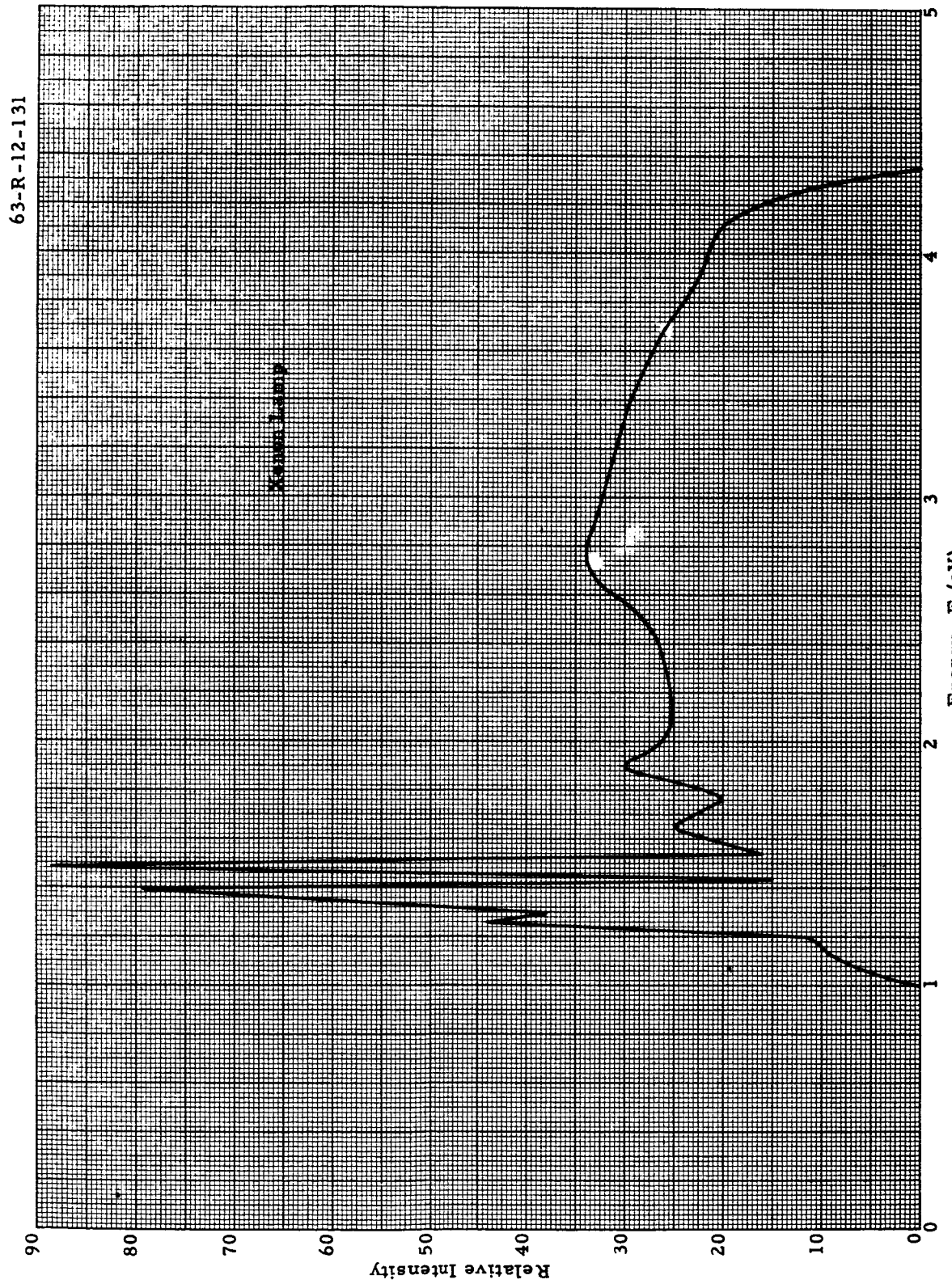

Figure 11. Xenon Lamp Spectrum

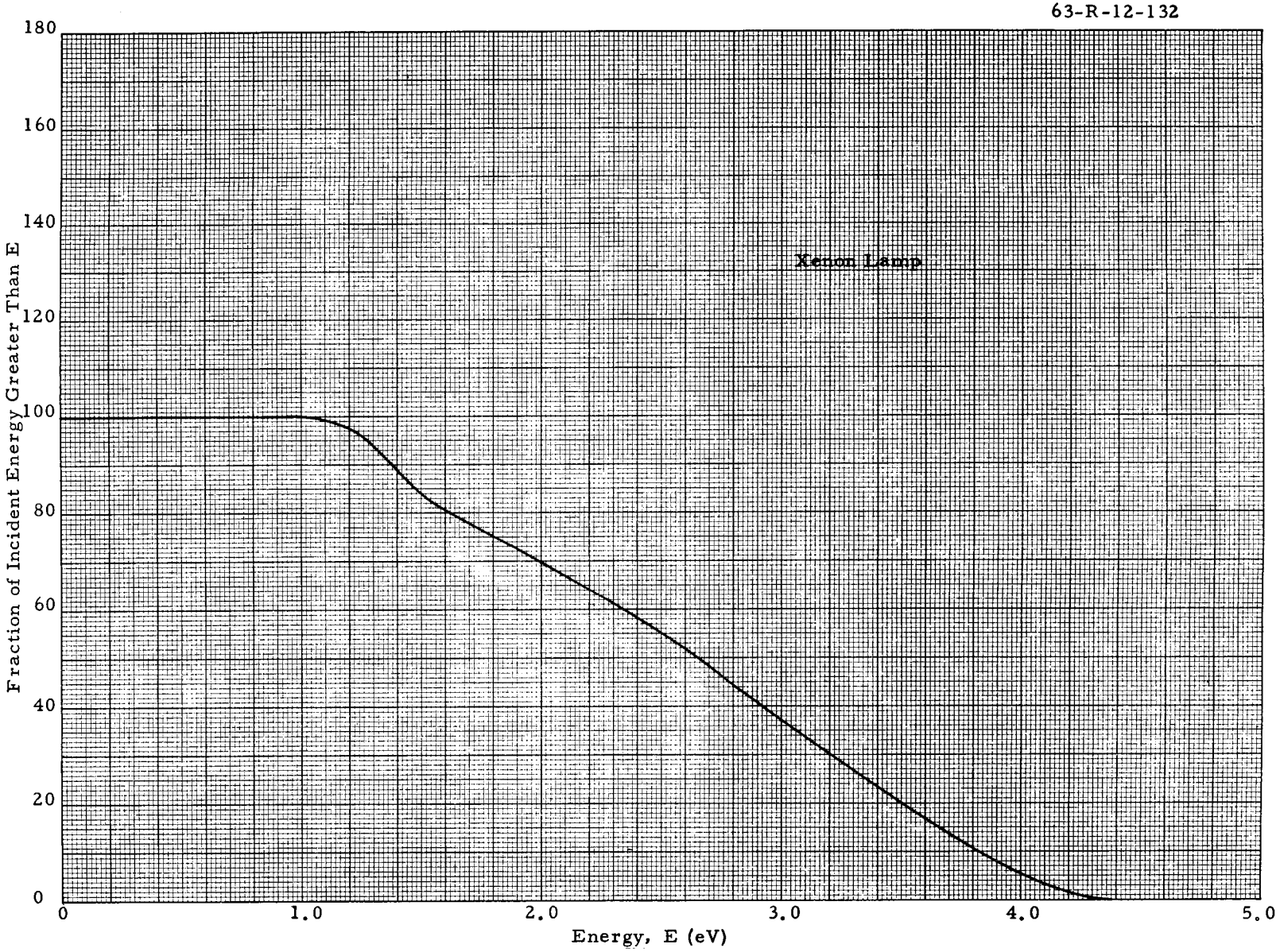

Figure 12. Integral of Xenon Lamp Spectrum

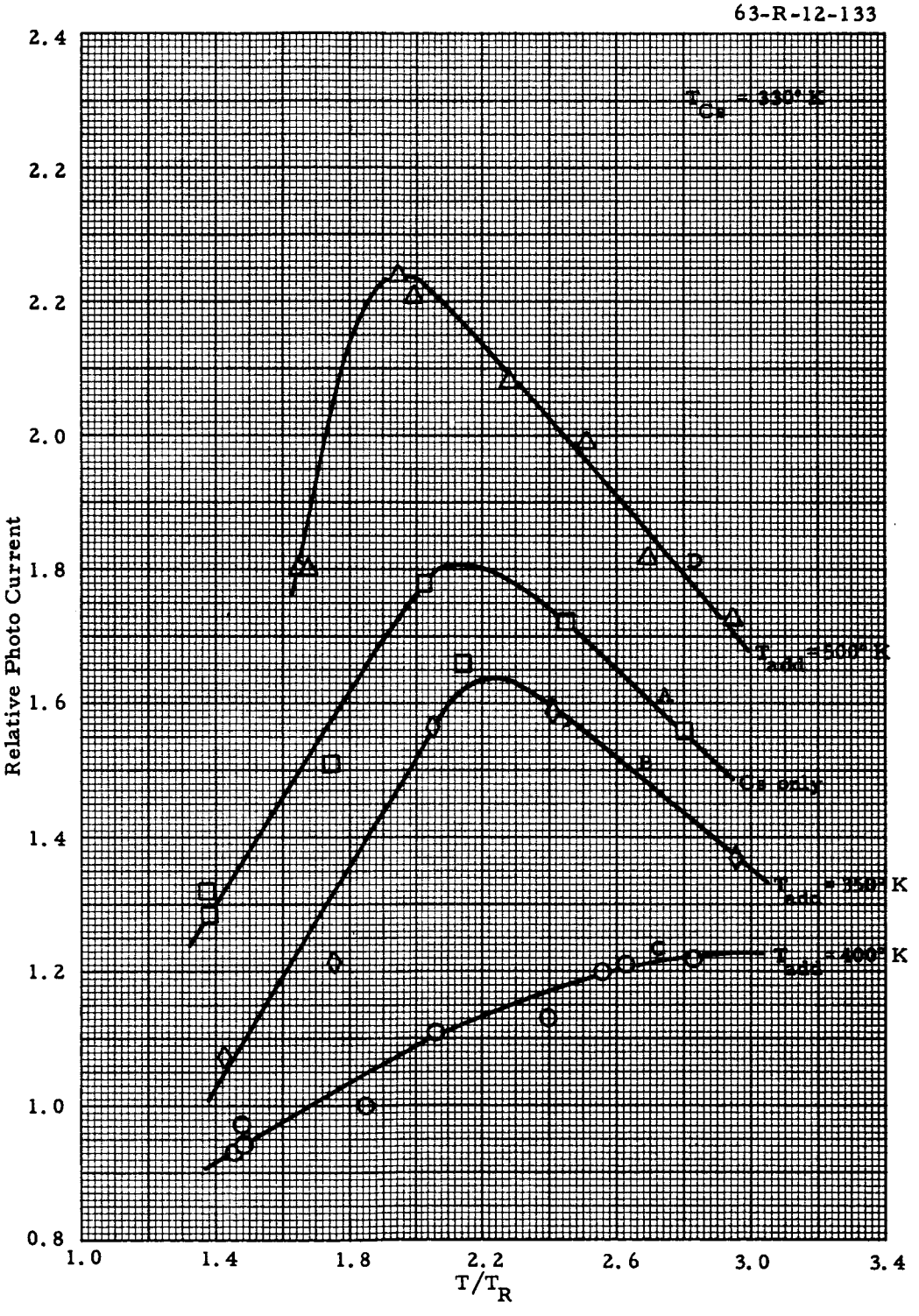

Figure 13. Relative Photo Current vs T/T_R

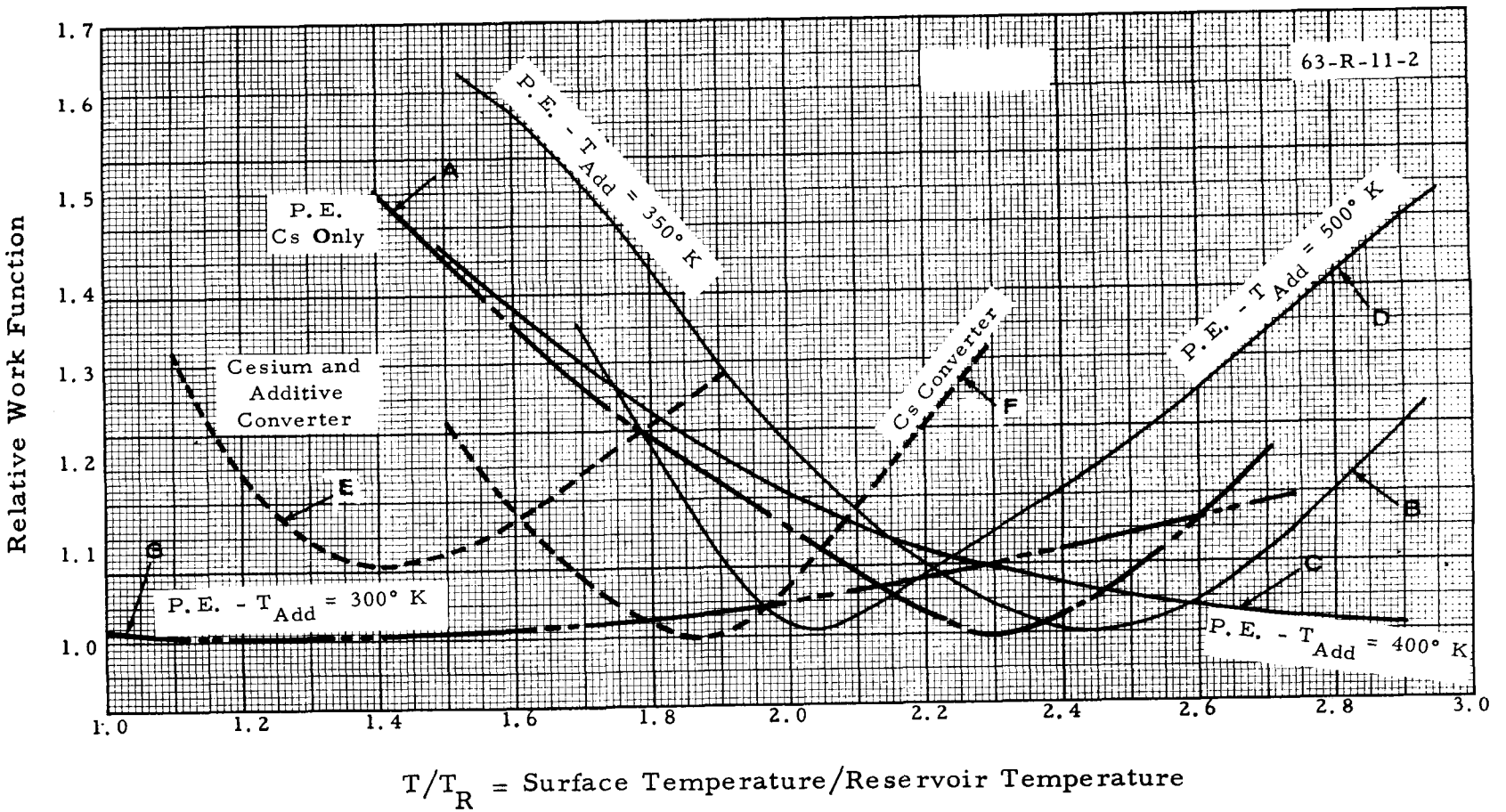

Figure 14. Relative ϕ_C vs. T/T_R

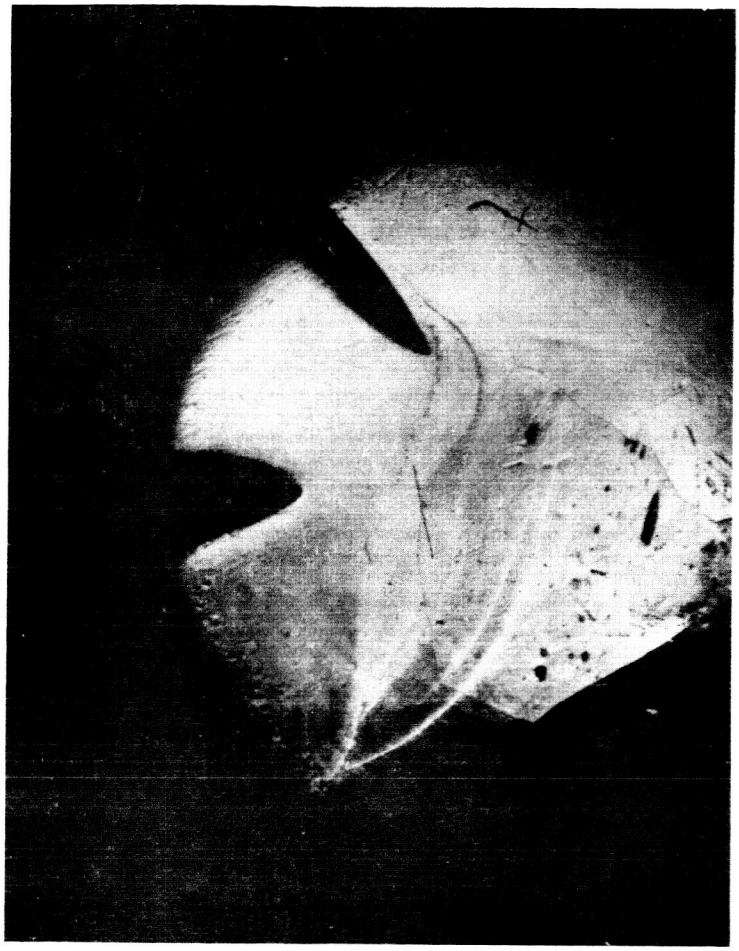

Figure 15. Photograph of Tungsten Emitter before Firing (5x)

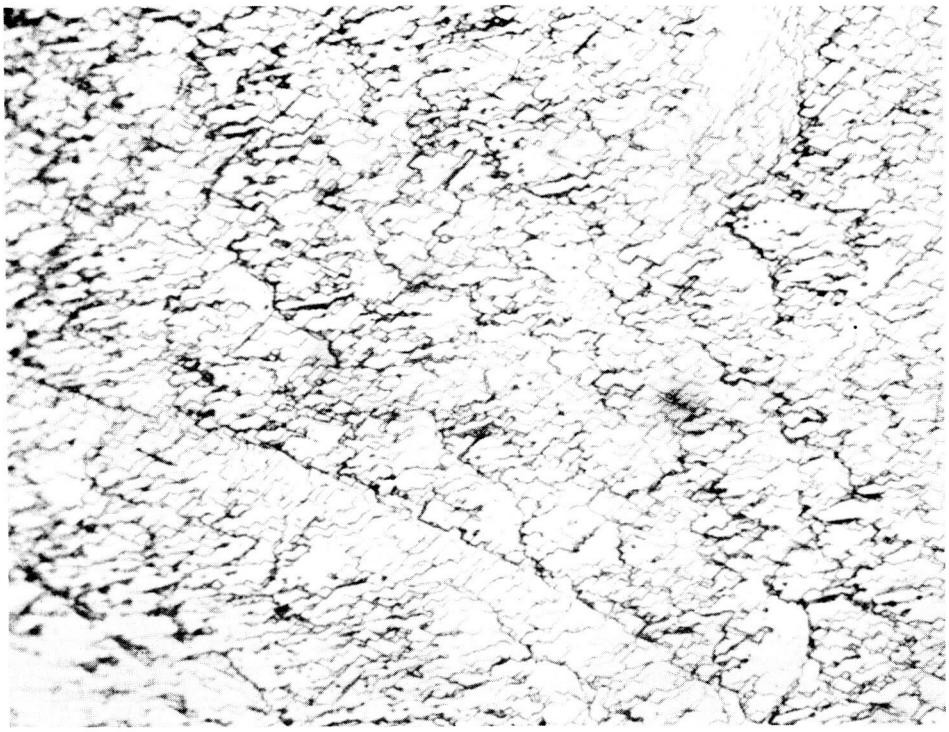

Figure 16. Photomicrograph of Tungsten Emitter before Firing

Figure 17. Photomicrograph of Tungsten Emitter after Firing (1085x)

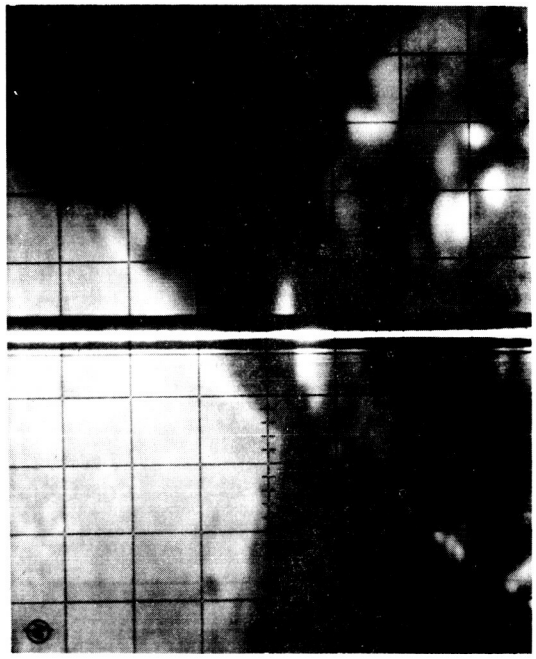

Figure 18. Thermionic Display Picture

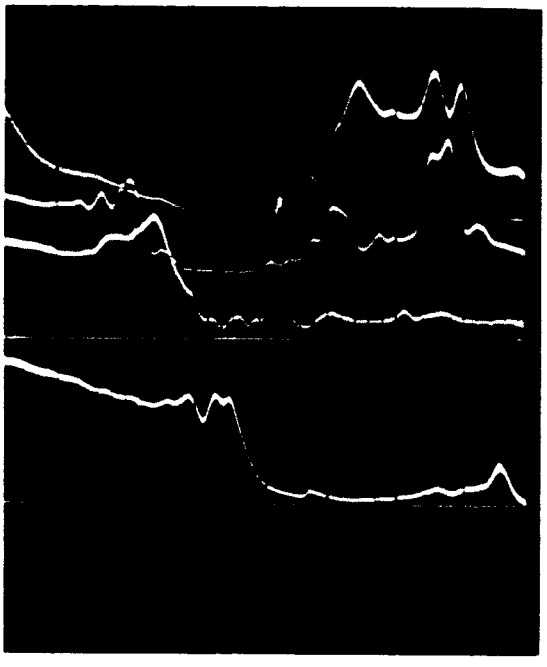

Figure 19. Thermionic Cross Scans of Four-Quadrant Emitter

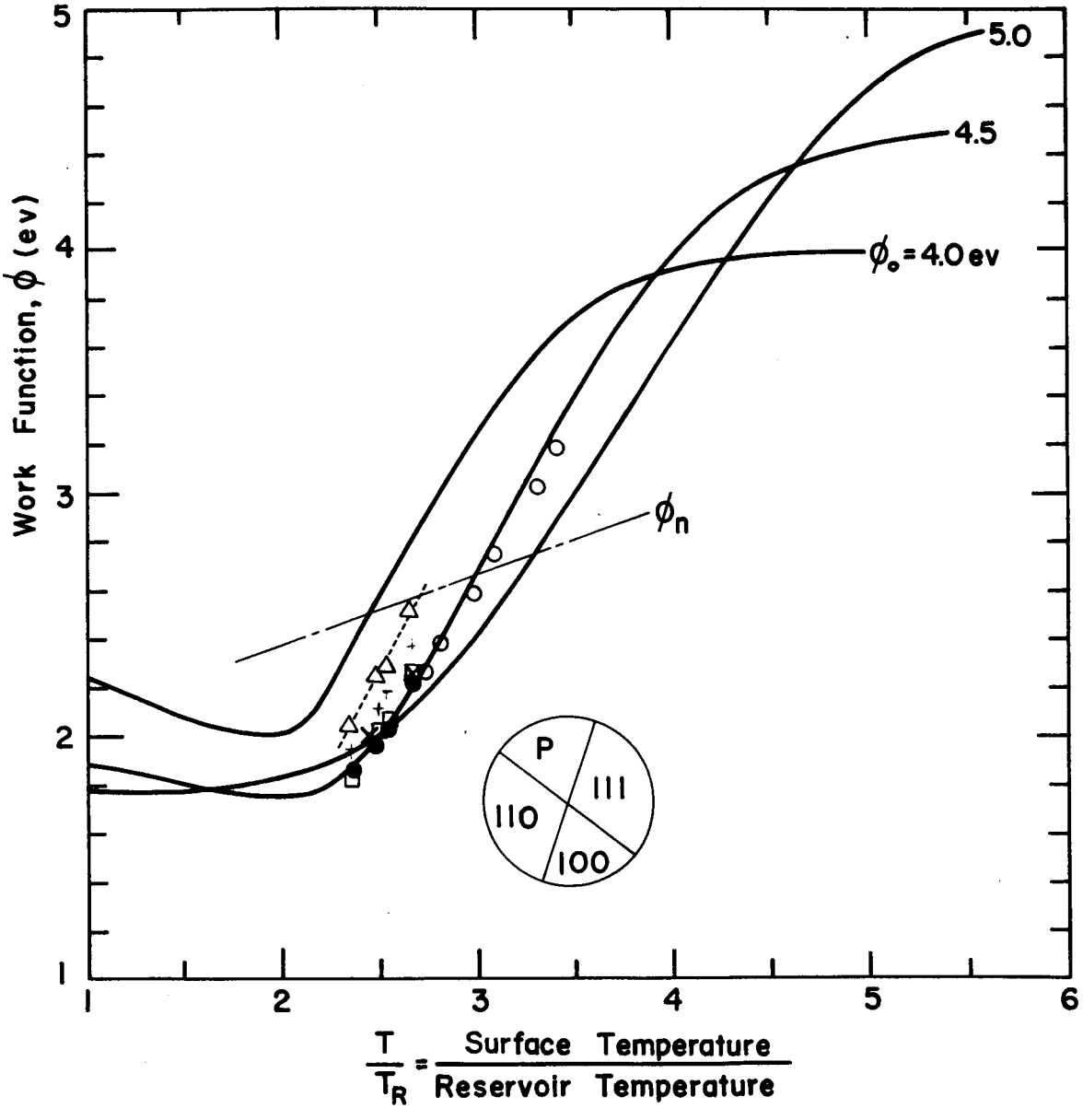

Figure 20. ϕ vs. T/T_R – Rasor Plots with Thermo Electron JPL Data Superimposed